Supplement of Ocean Sci., 21, 2179–2195, 2025
https://doi.org/10.5194/os-21-2179-2025-supplement

Ocean Science Open Access EGU

Supplement of

The coupled oxygen and carbon dynamics in the subsurface waters of the Gulf and Lower St. Lawrence Estuary and implications for artificial oxygenation

William A. Nesbitt et al.

Correspondence to: William A. Nesbitt (william.nesbitt@dal.ca)

S1 Extended Review of Previous Modeling Efforts

Savenkoff et al. (1996) assumed a homogenous, 150 m thick, deep layer with no significant vertical diffusion within the layer or across its upper boundary and applied the along-channel advection velocity of Bugden (1991; u = 5.0 × 10^{-3} m s^{-1}). They derived an oxygen utilization rate (OUR) estimate of 7 × 10^{-2} μmol O_2 m^{-2} s^{-1} (or 5.4 × 10^{-2} μmol C m^{-2} s^{-1}) from the DO gradient (ΔO/ΔC of 138/106) between two stations separated by ~570 km (Cabot Strait and Western GSL), attributing ~60% of the deep-layer dissolved oxygen (DO) depletion to the sediment oxygen demand (SOD) and the remainder to pelagic respiration in the bottom 150 m of the water column.

Benoit et al. (2006) employed a 2D coupled advection-diffusion-diagenetic model to constrain the oxygen budget in the deep layer of the Laurentian Channel (LC) along a 700 km horizontal transect. They applied the along-channel advection velocity proposed by Gilbert (2004; u = 1.0 × 10 m^{-2} s^{-1}) along with the diffusion coefficients of Bugden (1991; K_H = 8.2 × 10^2 m^2 s^{-1}, K_Z = 8.2 × 10^{-4} m^2 s^{-1}) and assumed that pelagic respiration was negligible. They reported OUR estimates for the bottom 100 m of the water column for two scenarios with differing organic matter fluxes: 2.7 × 10^{-2} μmol O_2 m^{-2} s^{-1} in the Gulf of St. Lawrence (GSL) and Lower St. Lawrence Estuary (LSLE) (low-flux scenario), and 2.7 × 10^{-2} μmol O_2 m^{-2} s^{-1} in the GSL increasing to >1.3 × 10^{-1} μmol O_2 m^{-2} s^{-1} in the LSLE (high-flux scenario).

Lehmann et al. (2009) measured the concentration and the stable oxygen isotope composition of DO in the water column of the LSLE and GSL and used a 1D diffusion-reaction model with an along-channel advection velocity of 1.0 × 10^{-2} m s^{-1} (Gilbert, 2004) to estimate the relative contribution of benthic and pelagic respiration on the OUR of the bottom 100 m of the LC. They estimated an average net community respiration rate of 1.74 × 10^{-1} μmol O_2 m^{-2} s^{-1} of which they attributed ~64% to SOD and ~36% to pelagic respiration.

Finally, Bourgault et al. (2012) revisited previous estimates (Benoit et al., 2006; Lehmann et al., 2009) using idealized, reverse 1D numerical simulations, historical DO observations and their mixing estimates based on flow turbulence measurements. Based on their model results, they concluded that pelagic, not benthic, respiration was the dominant oxygen sink in the bottom waters of the LSLE and GSL and this sink would have to be ~5x larger than the SOD, assuming a transit time between Cabot Strait and the head of the LSLE (~750 km) of 2.2 years (Gilbert, 2004; u = 1.0 × 10^{-2} m s^{-1}), or ~2x larger than the SOD for a transit time of 4.4 years (Bugden, 1991; u = 5.0 × 10^{-3} m s^{-1}). Bourgault et al. (2012) concluded that to maintain the observed conditions, K_Z would need to be << 1.0 × 10^{-4} m^2 s^{-1} for u = 1.0 × 10^{-2} m s^{-1} and << 5.0 × 10^{-5} m^2 s^{-1} for u = 5.0 × 10^{-3} m s^{-1}. They estimated an average OUR of 1.59 × 10^{-1} μmol O_2 m^{-2} s^{-1} for the bottom 100 m of the LC along a 750 km transect for an along-channel horizontal velocity of 1.0 × 10^{-2} m s^{-1}. The authors noted that using the advection velocity of Bugden (1991; 5.0 × 10^{-3} m s^{-1}), this rate would be 7.9 × 10^{-2} μmol O_2 m^{-2} s^{-1}. These OUR estimates were later reproduced by Jutras et al. (2020). Hence, previous OUR estimates (converted to μmol kg^{-1} yr^{-1}) vary widely due to inconsistencies in the dispersion parameters employed and are summarized in Table 1 in the main manuscript.

35 **S2 2021-2023 Station Coverage (TReX Program)**

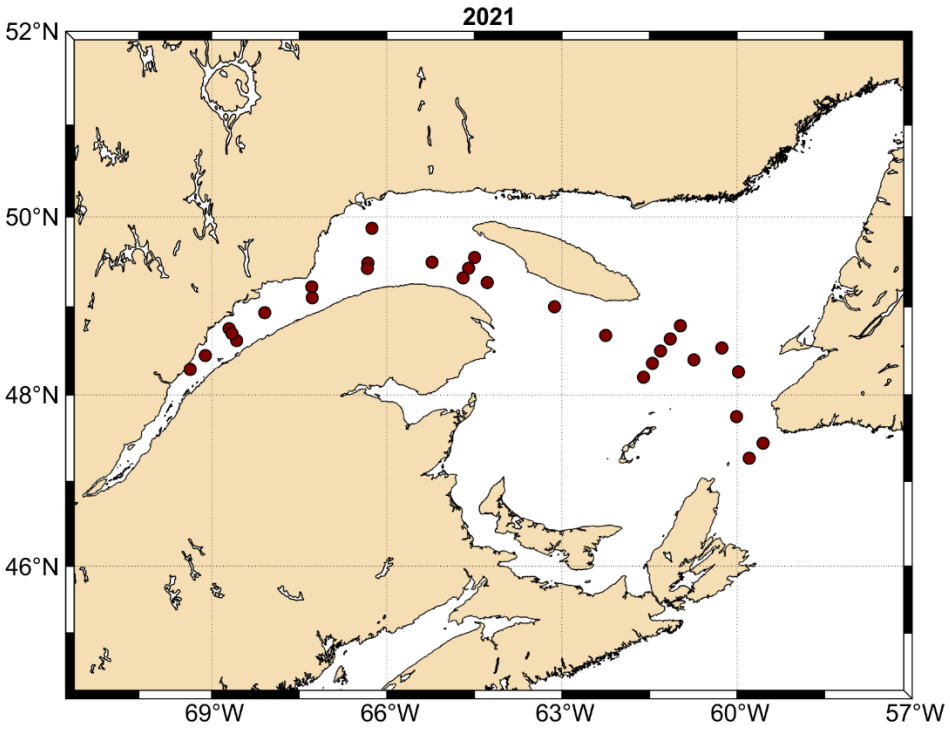

Figure S1: TReX program sampling stations along the Laurentian Channel for the year 2021 for which data were used in this study.

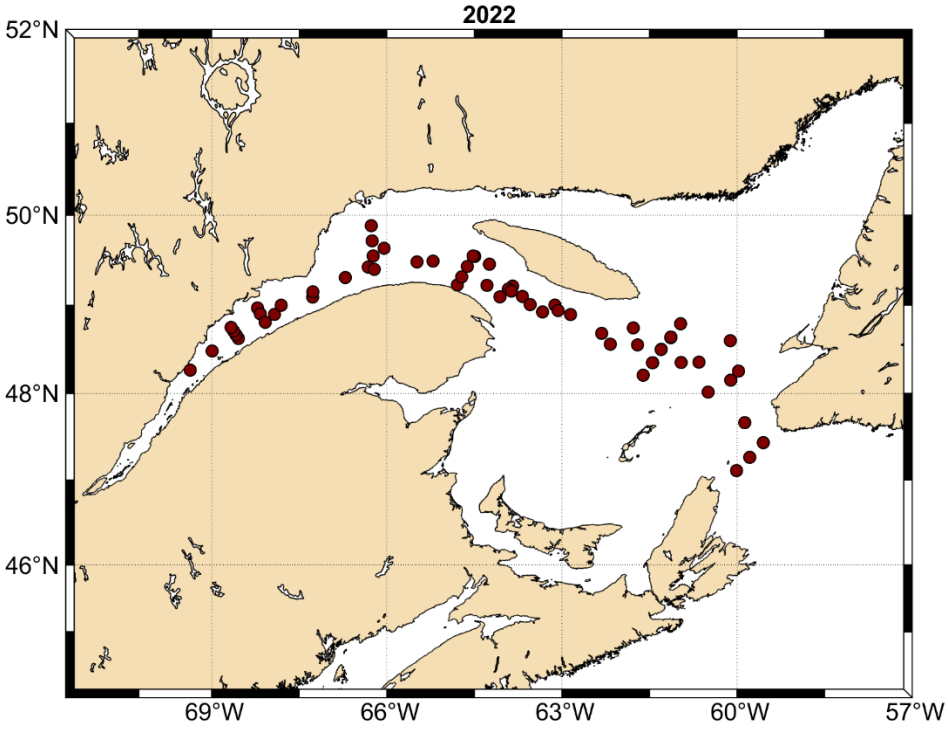

Figure S2: TReX program sampling stations along the Laurentian Channel for the year 2022 for which data were used in this study.

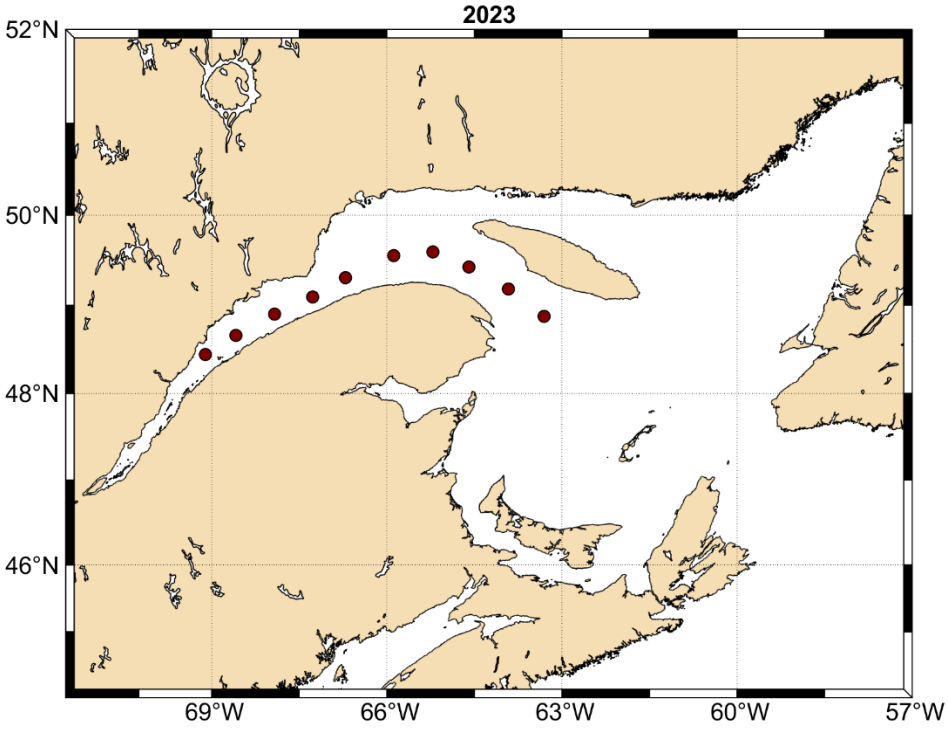

Figure S3: TReX program sampling stations along the Laurentian Channel for the year 2023 for which data were used in this study.

S3 Historical Data Set (2003-2020) Analytical Methods and Station Coverage

T and S_P were determined in situ using the rosette CTD probe. The conductivity probe was calibrated by the manufacturer over the winter prior to the cruises. In addition, the S_P of surface waters was determined by potentiometric argentometric titration at McGill University and calibration of the $AgNO_3$ titrant with IAPSO standard seawater. The reproducibility of these measurements is typically better than ± 0.5 %.

Water samples destined for A_T measurements were transferred to 250 mL glass bottles. They were poisoned with a few crystals of mercuric chloride ($HgCl_2$), and bottles sealed using a ground-glass stopper and Apiezon® Type-M high-vacuum grease. A_T was measured using an automated Radiometer (TitraLab865®) potentiometric titrator and a Red Rod® combination pH electrode (pHC2001) at McGill University. The diluted HCl titrant was calibrated prior, during and after each titration session using certified reference materials (CRMs) provided by Andrew Dickson (Scripps Institution of Oceanography). Raw titration data were processed with a proprietary algorithm designed for shallow endpoint detection. Based on replicate analyses of the same samples and CRMs, the reproducibility of the measurements was better than 0.1 %.

DO concentrations were determined on board by Winkler titration on distinct water samples recovered directly from the Niskin bottles, following the method described by (Grasshoff et al., 2009). The relative standard deviation, based

on replicate analyses of samples recovered from the same Niskin bottle, was 0.5 %. These measurements served to calibrate the SBE-43 oxygen probe mounted on the rosette sampler.

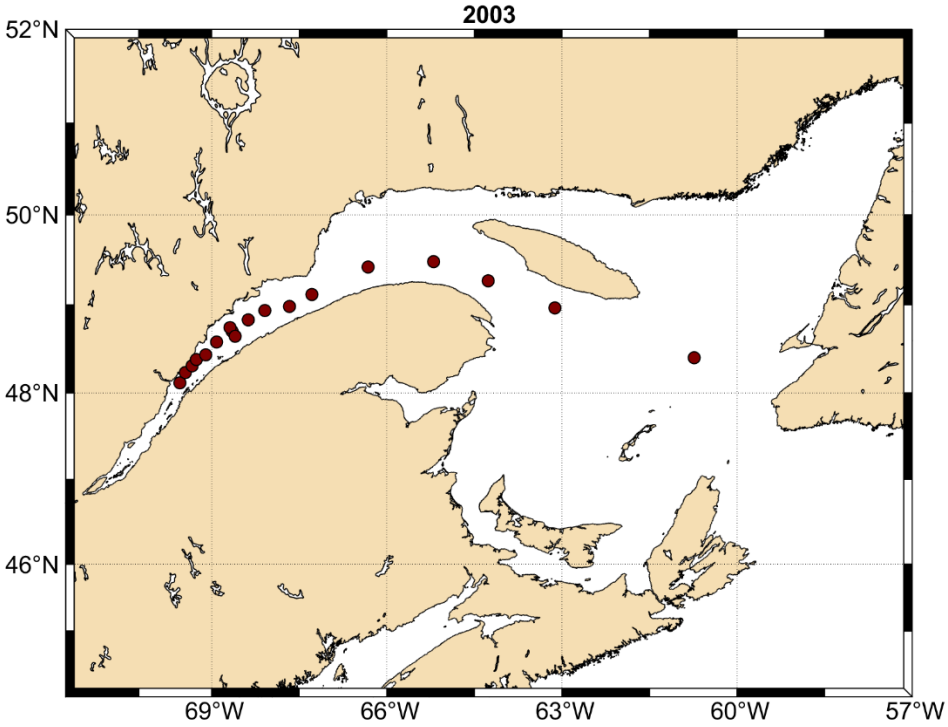

Figure S4: Sampling stations along the Laurentian Channel for the year 2003 for which data were used in this study.

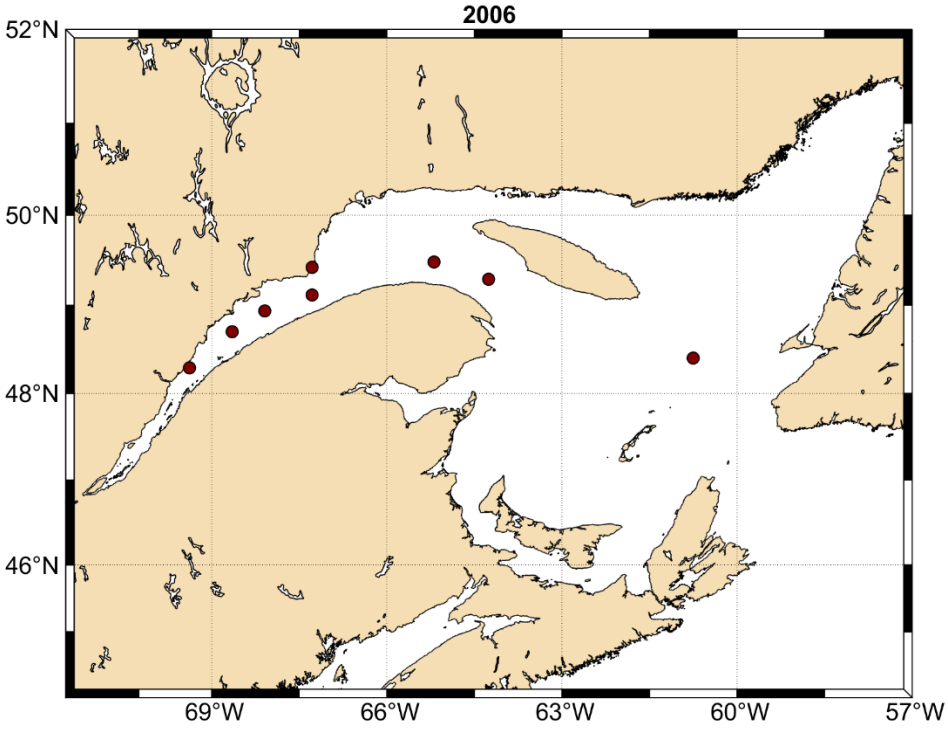

Figure S5: Sampling stations along the Laurentian Channel for the year 2006 for which data were used in this study.

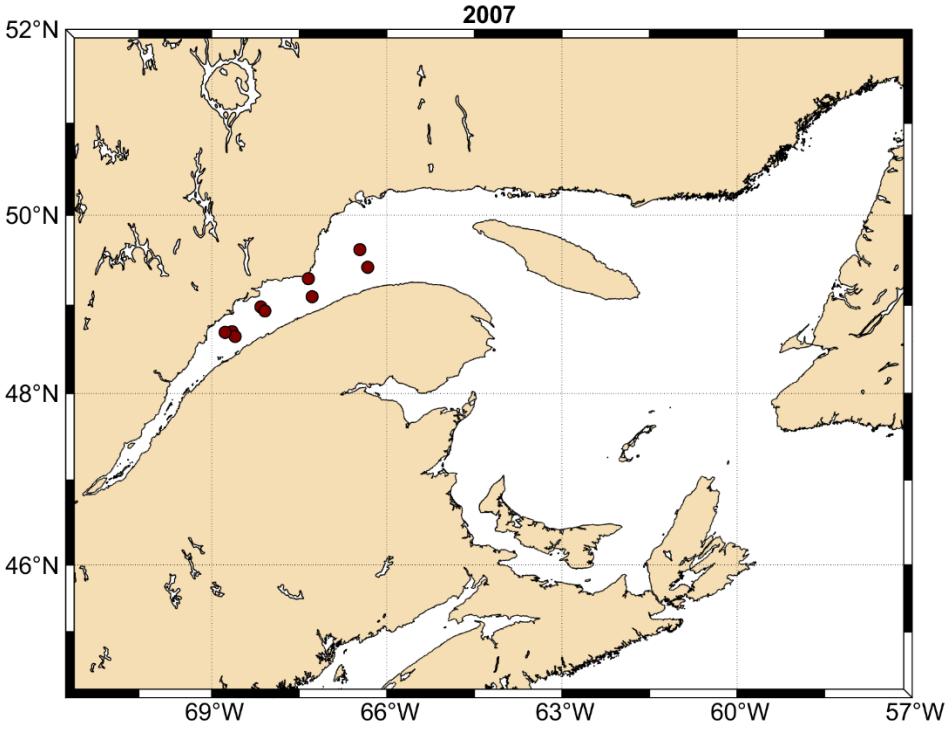

Figure S6: Sampling stations along the Laurentian Channel for the year 2007 for which data were used in this study.

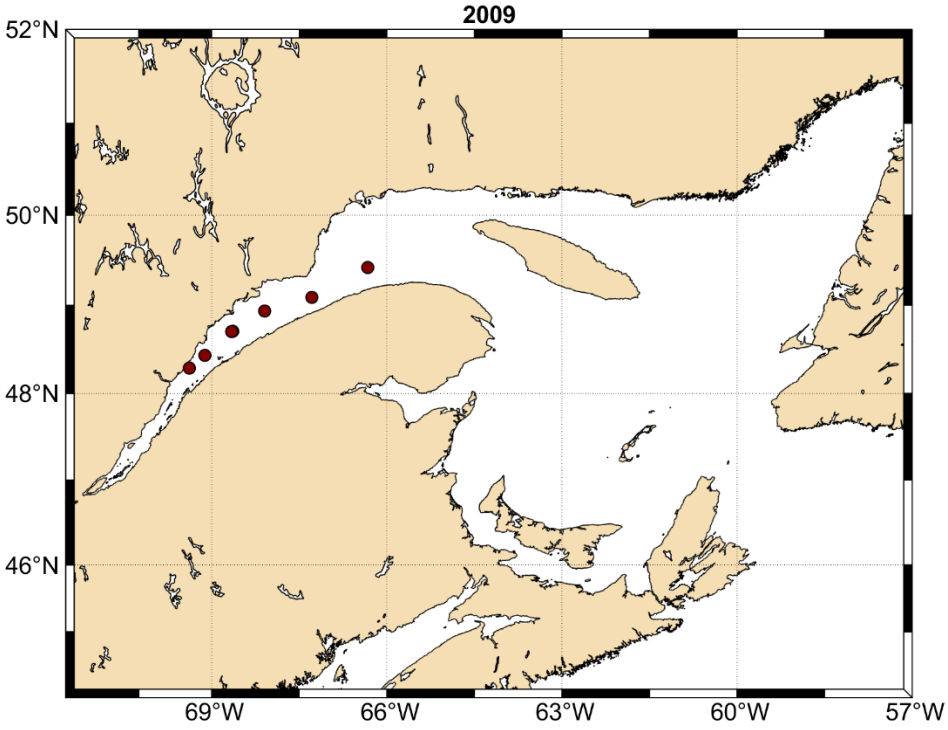

Figure S7: Sampling stations along the Laurentian Channel for the year 2009 for which data were used in this study.

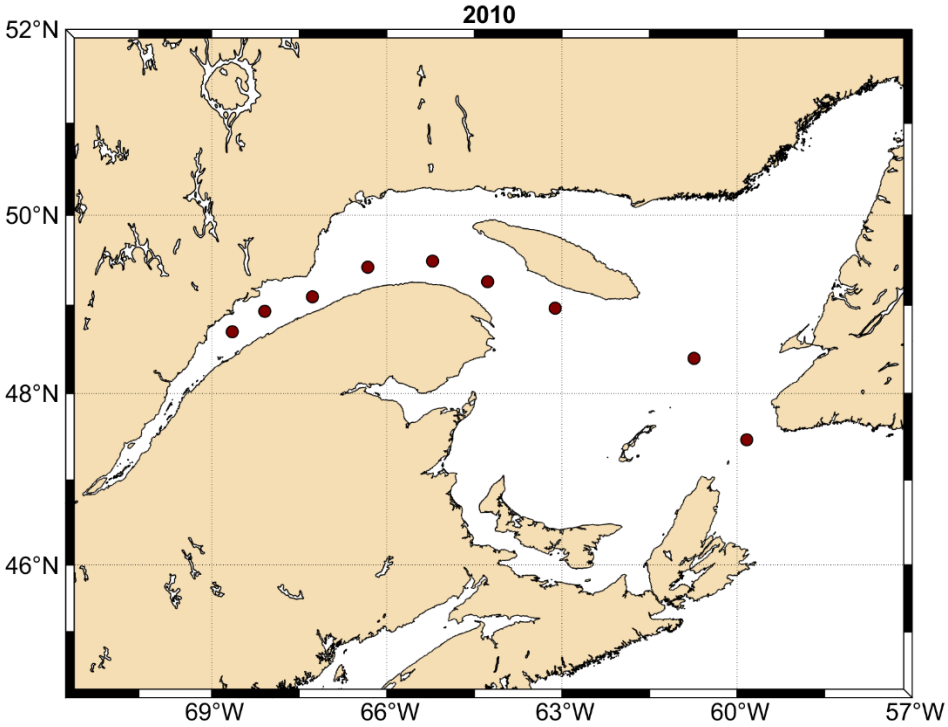

70

Figure S8: Sampling stations along the Laurentian Channel for the year 2010 for which data were used in this study.

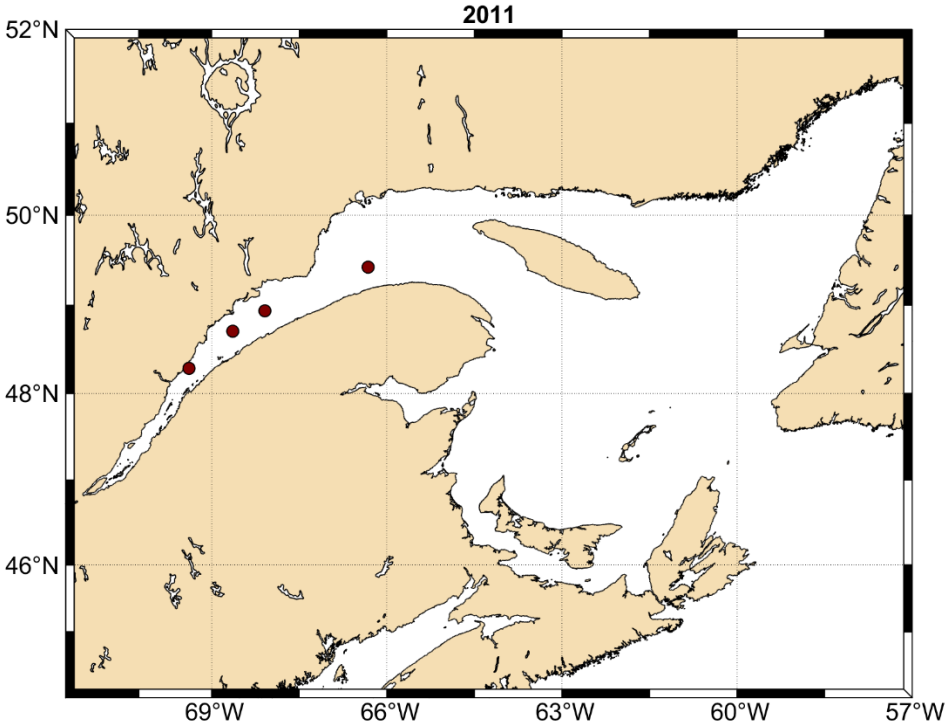

Figure S9: Sampling stations along the Laurentian Channel for the year 2011 for which data were used in this study.

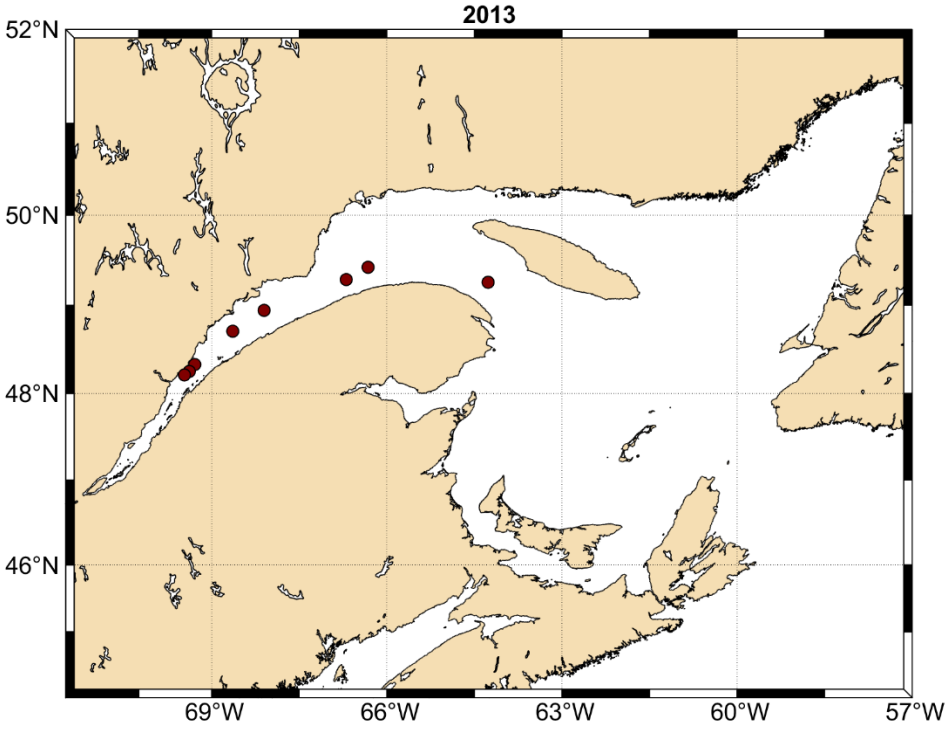

Figure S10: Sampling stations along the Laurentian Channel for the year 2013 and which data were used in this study.

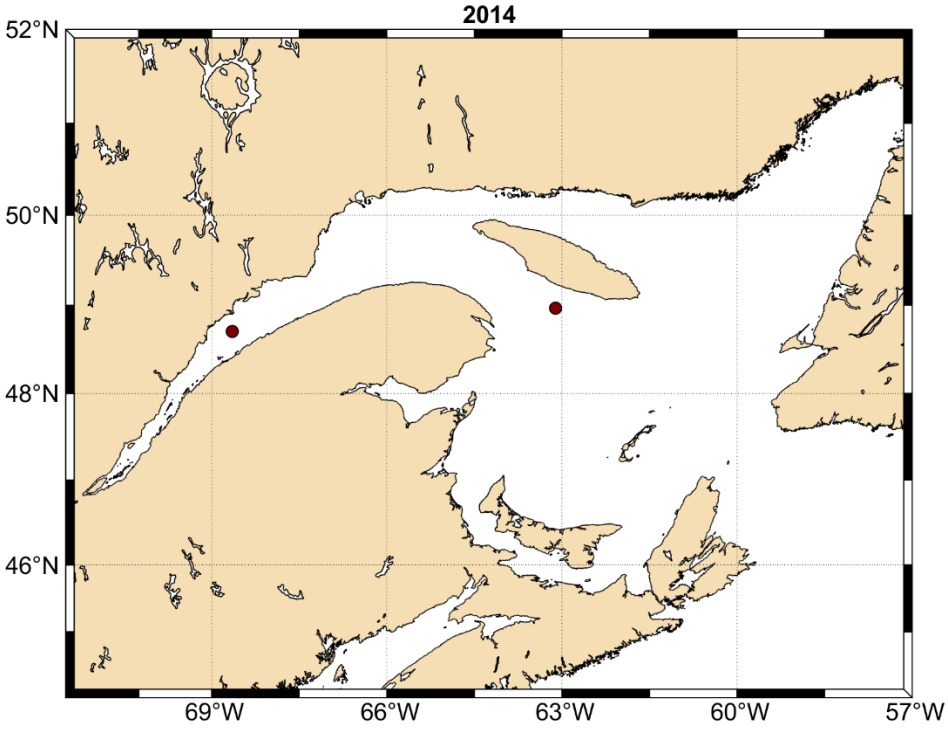

Figure S11: Sampling stations along the Laurentian Channel for the year 2014 for which data were used in this study.

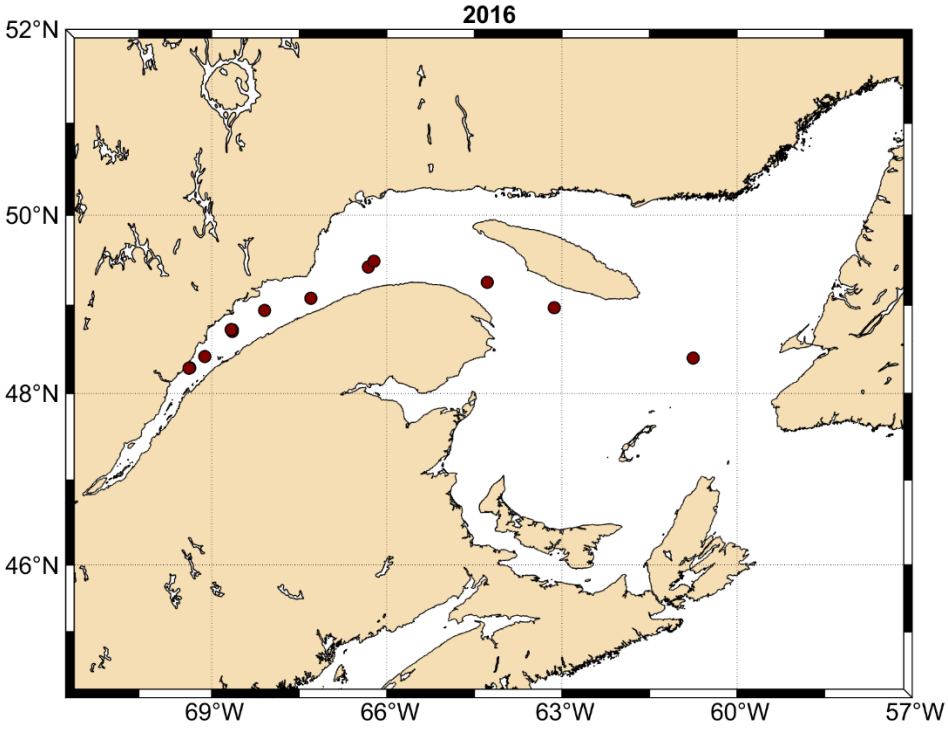

Figure S12: Sampling stations along the Laurentian Channel for the year 2016 for which data were used in this study.

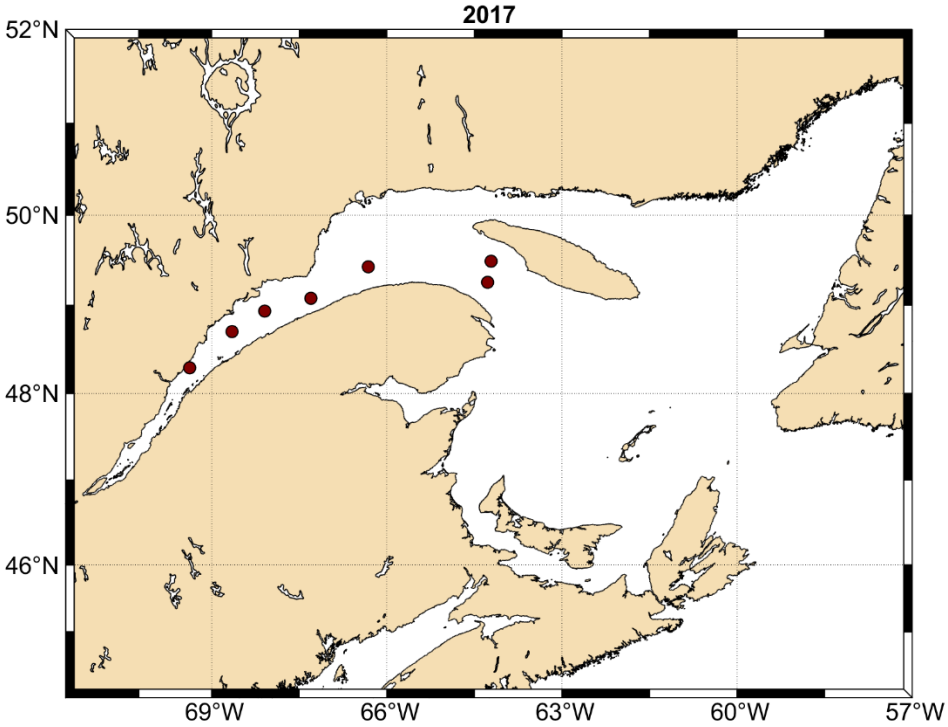

80

Figure S13: Sampling stations along the Laurentian Channel for the year 2017 for which data were used in this study.

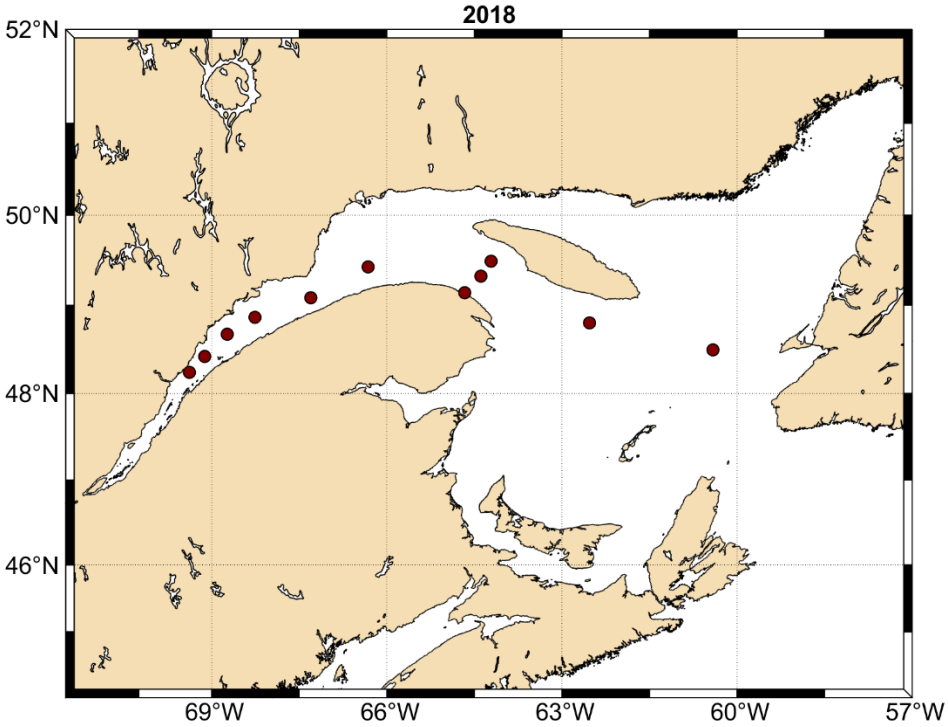

Figure S14: Sampling stations along the Laurentian Channel for the year 2018 for which data were used in this study.

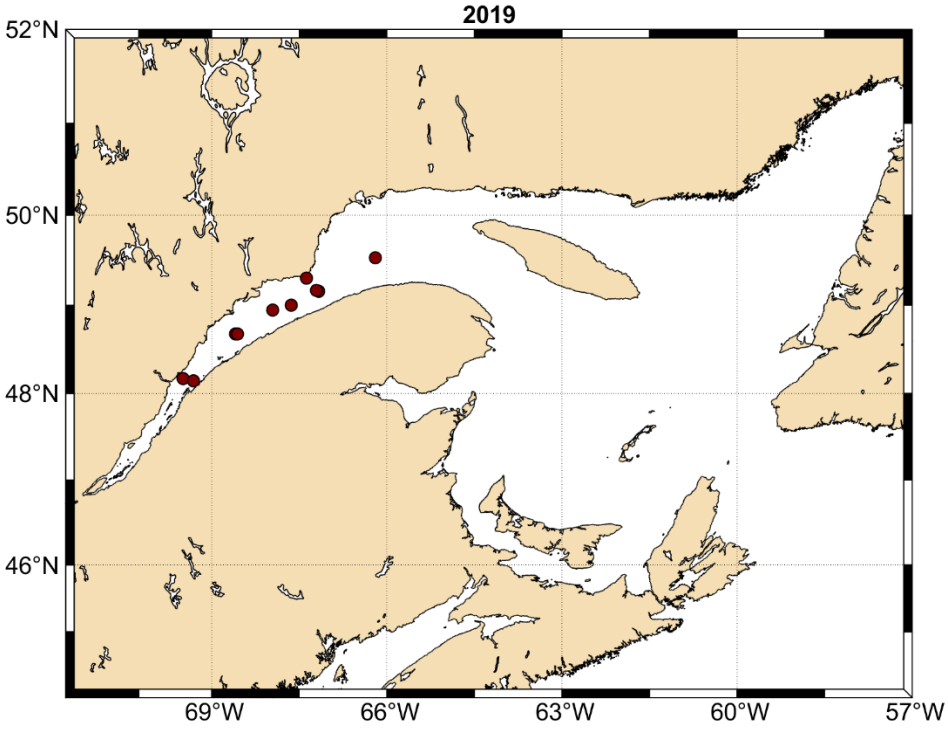

Figure S15: Sampling stations along the Laurentian Channel for the year 2019 for which data were used in this study.

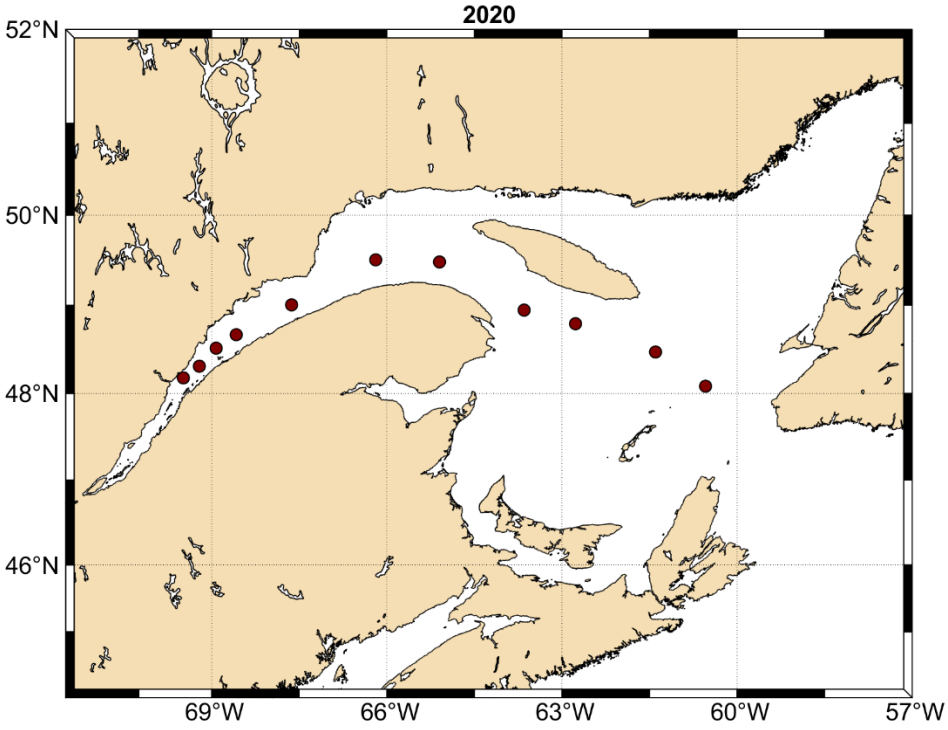

Figure S16: Sampling stations along the Laurentian Channel for the year 2020 for which data were used in this study.

90

95

S4 Inflow Boundary Condition Estimations (along-channel regressions)

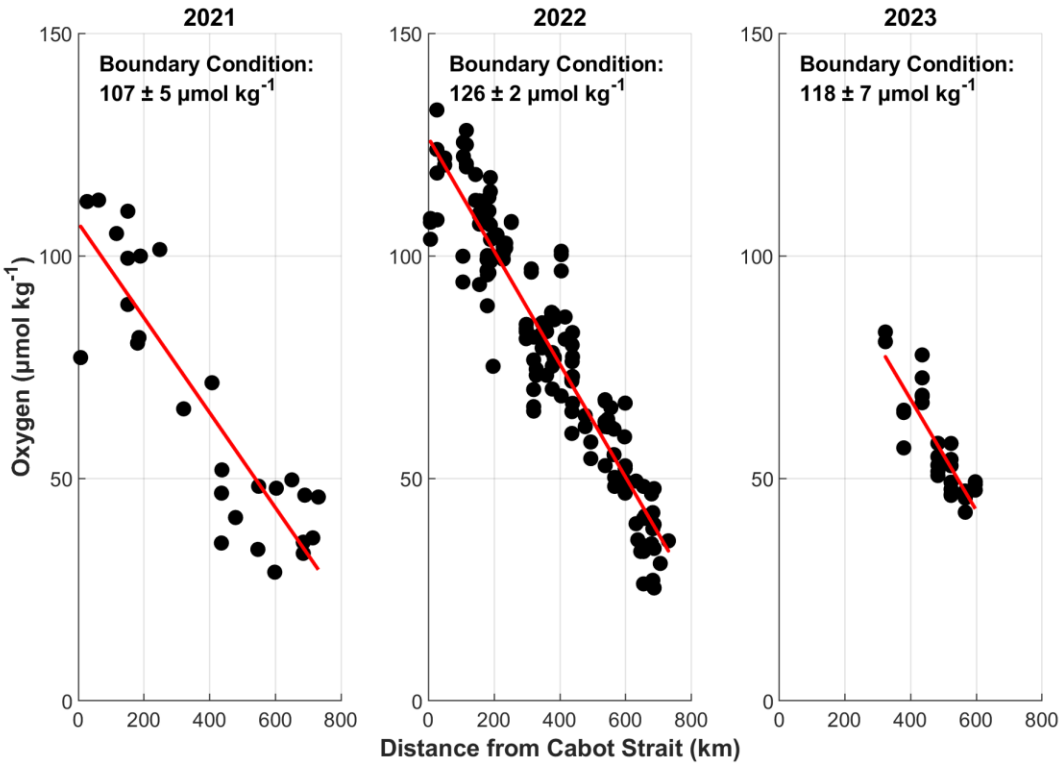

100

Figure S17: Along-channel regressions of dissolved oxygen concentrations between the 27.15 and 27.30 kg m^{-3} isopycnals over the distance from Cabot Strait. Boundary conditions for each year (2021-2023) are derived from the intercepts at Cabot Strait (0 km).

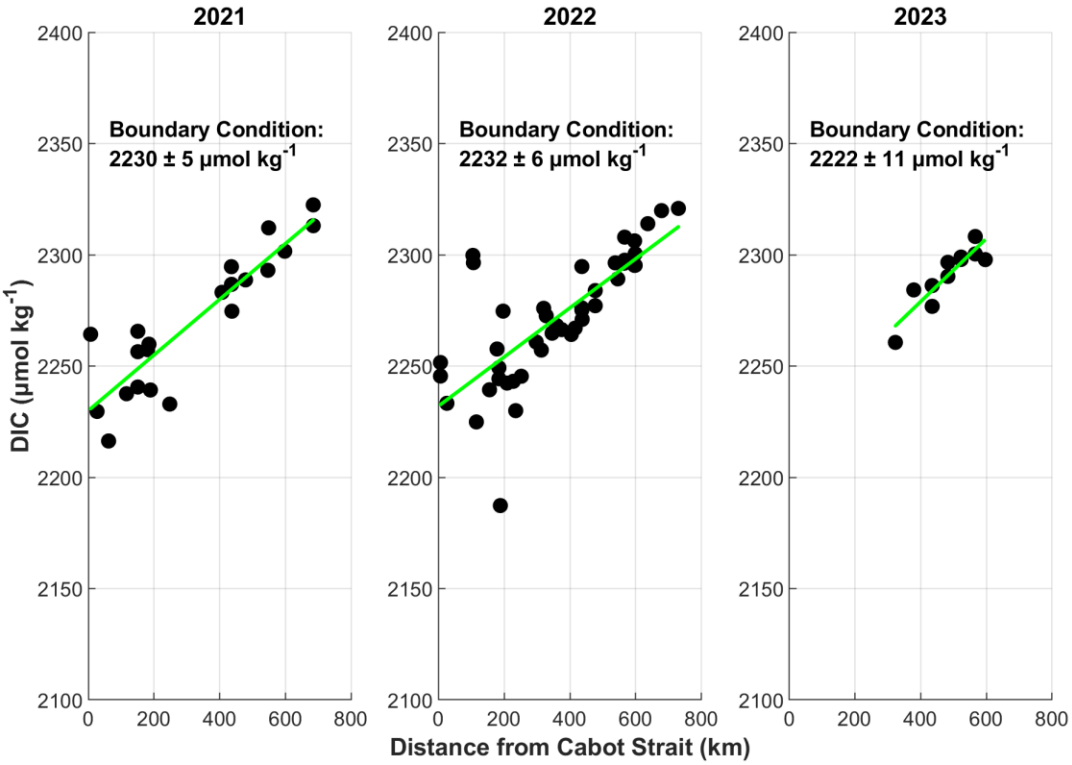

105 **Figure S18: Along-channel regressions of DIC concentrations between the 27.15 and 27.30 kg m^{-3} isopycnals over the distance from Cabot Strait. Boundary conditions for each year (2021-2023) are derived from the intercepts at Cabot Strait (0 km).**

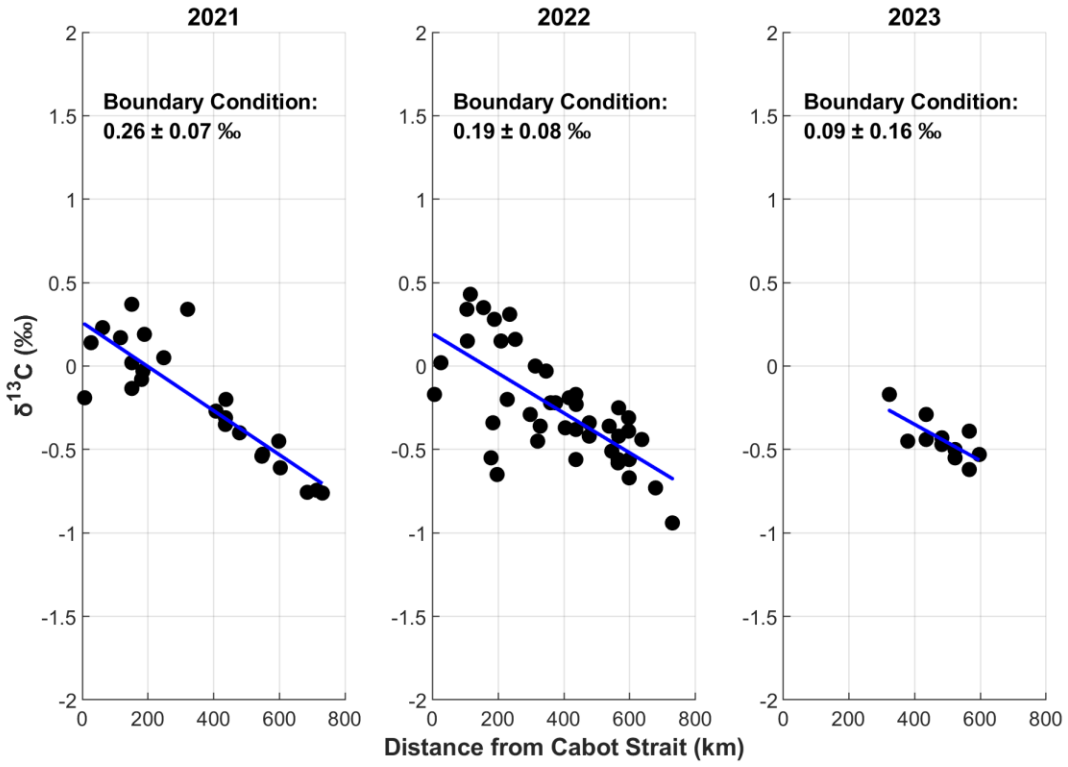

Figure S19: Along-channel regressions of $\delta^{13}C_{DIC}$ composition between the 27.15 and 27.30 kg m^{-3} isopycnals over the distance from Cabot Strait. Boundary conditions for each year (2021-2023) are derived from the intercepts at Cabot Strait (0 km).

S5 1D Model Boundary Conditions and LS Fit S Terms

Table S1: Boundary condition oxygen concentrations (± standard deviation, µmol kg^{-1}), fitted source terms (S, µmol kg^{-1} s^{-1}), and corresponding Oxygen Utilization Rates (OUR, µmol kg^{-1} yr^{-1}) derived from the advection-diffusion model least-squares fit to observed dissolved oxygen concentrations along the Laurentian Channel for the period 2003–2023. Blank entries indicate years where data were unavailable.

Year	Boundary Condition	Source Term (S)	OUR
1999	162 ± 19		
2000	177 ± 15		
2001	145 ± 17		
2002	155 ± 10		
2003	150 ± 10	-7.71×10^{-7}	24.32
2004	141 ± 7		
2005	127 ± 44		
2006	166 ± 19	-6.35×10^{-7}	20.03
2007	146 ± 16	-5.23×10^{-7}	16.48
2008	165 ± 11		
2009	156 ± 9	-7.18×10^{-7}	22.64
2010	156 ± 13	-6.73×10^{-7}	21.22
2011	156 ± 6	-7.22×10^{-7}	22.76
2012	174		
2013	151 ± 9	-7.03×10^{-7}	22.16
2014	154 ± 15	-7.40×10^{-7}	23.33
2015	142 ± 1		
2016	147	-6.61×10^{-7}	20.85
2017	143 ± 9	-7.87×10^{-7}	24.83
2018	126 ± 5	-7.16×10^{-7}	22.59
2019	125 ± 6	-6.74×10^{-7}	21.25
2020	110	-6.33×10^{-7}	19.97
2021	107 ± 5	-6.83×10^{-7}	21.54
2022	127 ± 2	-5.21×10^{-7}	16.42
2023	118 ± 7	-5.66×10^{-7}	17.84
Mean			**21.14 ± 2.43**

Table S2: Boundary condition dissolved inorganic carbon (DIC) concentrations (µmol kg^{-1}), derived source terms (S, µmol kg^{-1} s^{-1}), and corresponding annual DIC accumulation rates (µmol kg^{-1} yr^{-1}) from advection-diffusion model least-squares fit for the years 2021–2023.

Year	Boundary Condition	Source Term (S)	DIC Accumulation Rate
2021	2230 ± 5	6.32×10^{-7}	19.92
2022	2232 ± 6	4.68×10^{-7}	14.75
2023	2222 ± 11	6.37×10^{-7}	20.09
Mean			**18.25 ± 2.48**

Table S3. Boundary condition stable carbon isotope ($\delta^{13}C_{DIC}$) values (‰), derived source terms (S, ‰ kg^{-1} s^{-1}), and corresponding annual $\delta^{13}C_{DIC}$ dilution rates (‰ yr^{-1}) from advection-diffusion model least-squares fit for the years 2021–2023.

Year	Boundary Condition	Source Term (S)	$\delta^{13}C_{DIC}$ Dilution Rate
2021	0.26 ± 0.07	-6.67×10^{-9}	0.21
2022	0.19 ± 0.08	-5.47×10^{-9}	0.17
2023	0.09 ± 0.16	-5.54×10^{-9}	0.17
Mean			**0.19 ± 0.02**

S6 – Temperature Analysis: Q_{10} and Linear Regression

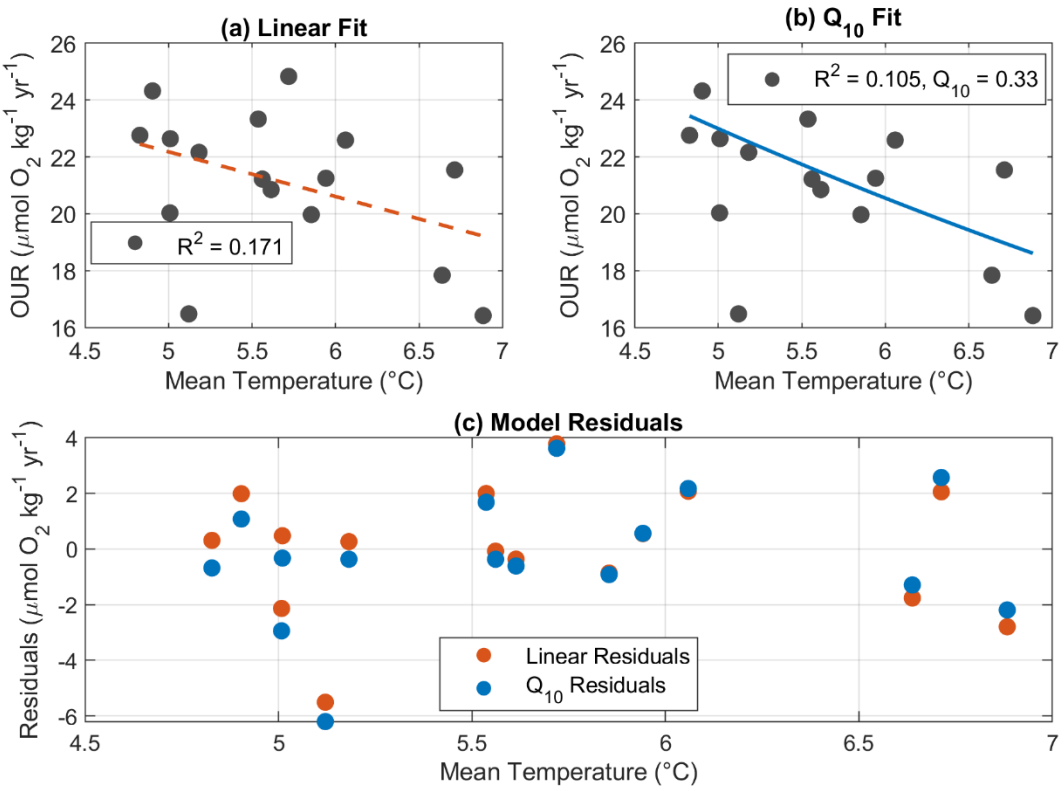

Figure S20: Comparison of modeled Oxygen Utilization Rate (OUR) as a function of mean temperature. (a) Linear least-squares regression fit with an R^2 value of 0.171, indicating a weak negative correlation between OUR and mean temperature. (b) Q_{10} model fit with an R^2 value of 0.105 and a Q_{10} value of 0.33, suggesting a similarly weak temperature dependence. (c) Model residuals for both the linear (orange) and Q_{10} (blue) fits, highlighting the deviations between the observed and predicted OUR values. The low R^2 values suggest limited influence of temperature on interannual OUR variability.

S7 A_T/S_P Linear Regression for 2021-2023 TReX Data

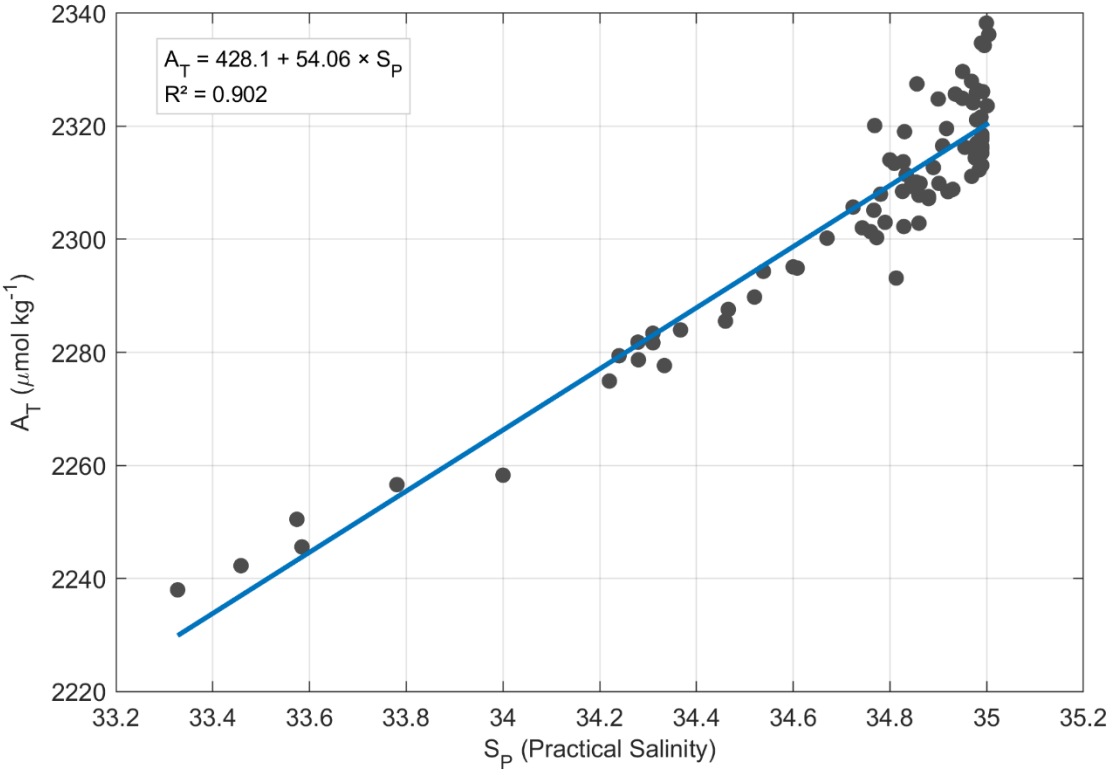

Figure S21. Linear relationship between total alkalinity (A_T) and practical salinity (S_P) for the Laurentian Channel (data from the 2021-2023 TReX Program). The fitted linear regression is described by $A_T = 428.1 + 54.06 \times S_P$ with an R^2 value of 0.902. This relationship suggests that S_P is the dominant driver of A_T variability in the deep layer. At high salinity (>34.7), a distinct "hockey stick shape" emerges, which could be attributed to a change in the dominant water mass entering through the Cabot Strait in ~2020, possibly influenced by a shift in the end-member composition (Jutras et al., 2020, 2023a, b).

S8 Model Sensitivity to spatial heterogeneity in OUR

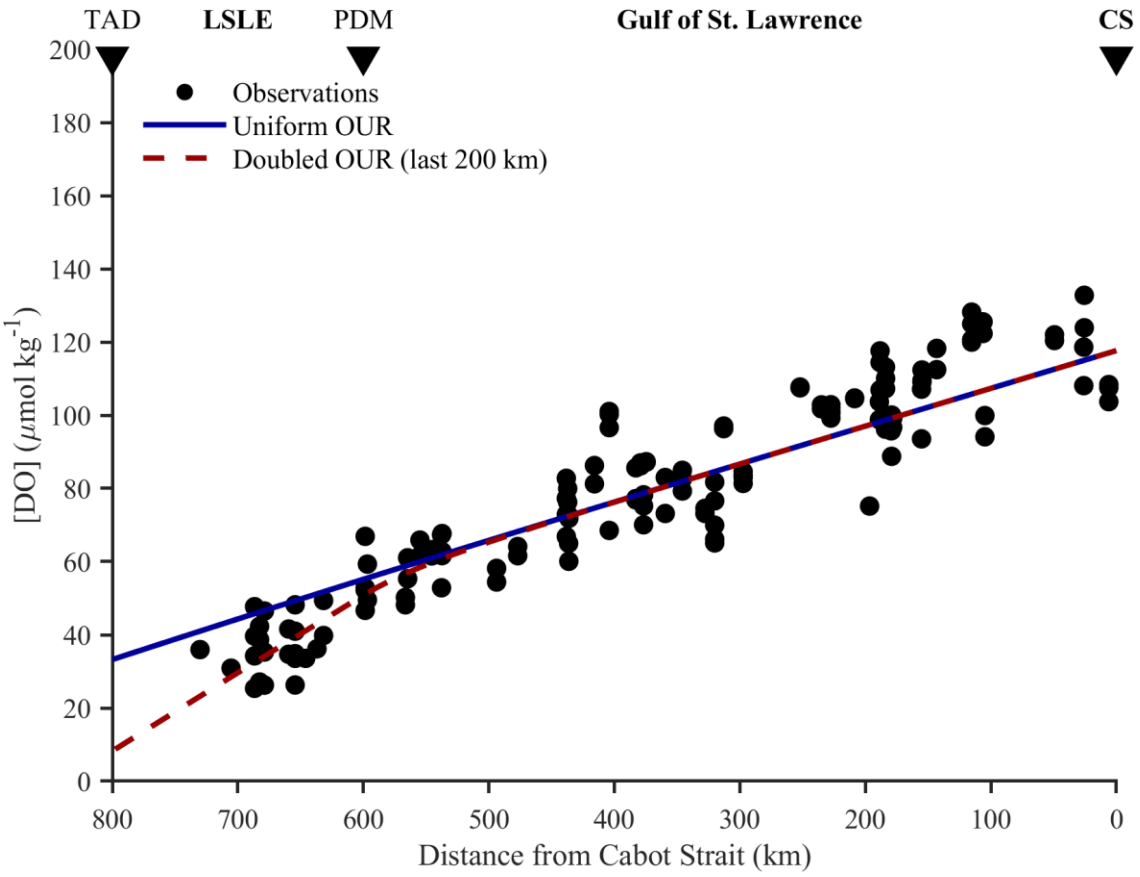

Figure S22: Sensitivity of the 1D advection-diffusion model to spatial variability in the oxygen utilization rate (OUR). The model is initialized with observed deepwater O_2 concentrations at Cabot Strait and run forward with either a spatially uniform OUR (solid blue line; fit to observations from 2022 (black dots)) or a doubled OUR in the inner 200 km of the Laurentian Channel (dashed red line), approximating elevated remineralization in the LSLE where the supply of allochthonous OM is enhanced. Regional labels highlight key longitudinal transitions along the Laurentian Channel: TAD = Tadoussac, LSLE = Lower St. Lawrence Estuary, PDM = Pointe-des-Monts, and CS = Cabot Strait. The spatial pattern of [DO] is well captured in both cases, with the doubled-OUR scenario yielding only a ~2% decrease in misfit.

References

Benoit, P., Gratton, Y., and Mucci, A.: Modeling of dissolved oxygen levels in the bottom waters of the Lower St. Lawrence Estuary: Coupling of benthic and pelagic processes, Marine Chemistry, 102, 13–32, https://doi.org/10.1016/j.marchem.2005.09.015, 2006.

Bourgault, D., Cyr, F., Galbraith, P. S., and Pelletier, E.: Relative importance of pelagic and sediment respiration in causing hypoxia in a deep estuary, Journal of Geophysical Research: Oceans, 117, https://doi.org/10.1029/2012JC007902, 2012.

Bugden, G. L.: Changes in the temperature-salinity characteristics of the deeper waters of the Gulf of St. Lawrence over the past few decades, Can. J. Fish. Aquat. Sci., 113, 139–147, 1991.

Gilbert, D.: Propagation of Temperature Signals from the Northwest Atlantic Continental Shelf Edge into the Laurentian Channel, in: ICES Council Meeting, ICES Council Meeting, 2004.

Grasshoff, K., Kremling, K., and Ehrhardt, M.: Methods of Seawater Analysis, 3rd ed., John Wiley & Sons, Weinheim, Germany, 635 pp., 2009.

Jutras, M., Dufour, C. O., Mucci, A., Cyr, F., and Gilbert, D.: Temporal Changes in the Causes of the Observed Oxygen Decline in the St. Lawrence Estuary, Journal of Geophysical Research: Oceans, 125, e2020JC016577, https://doi.org/10.1029/2020JC016577, 2020.

Jutras, M., Dufour, C. O., Mucci, A., and Talbot, L. C.: Large-scale control of the retroflection of the Labrador Current, Nat Commun, 14, 2623, https://doi.org/10.1038/s41467-023-38321-y, 2023a.

Jutras, M., Mucci, A., Chaillou, G., Nesbitt, W. A., and Wallace, D. W. R.: Temporal and spatial evolution of bottom-water hypoxia in the St Lawrence estuarine system, Biogeosciences, 20, 839–849, https://doi.org/10.5194/bg-20-839-2023, 2023b.

Lehmann, M. F., Barnett, B., Gélinas, Y., Gilbert, D., Maranger, R. J., Mucci, A., Sundby, B., and Thibodeau, B.: Aerobic respiration and hypoxia in the Lower St. Lawrence Estuary: Stable isotope ratios of dissolved oxygen constrain oxygen sink partitioning, Limnology and Oceanography, 54, 2157–2169, https://doi.org/10.4319/lo.2009.54.6.2157, 2009.

Savenkoff, C., Vézina, A. F., Packard, T. T., Silverberg, N., Therriault, J.-C., Chen, W., Bérubé, C., Mucci, A., Klein, B., Mesplé, F., Tremblay, J.-E., Legendre, L., Wesson, J., and Ingram, R. G.: Distributions of oxygen, carbon, and respiratory activity in the deep layer of the Gulf of St. Lawrence and their implications for the carbon cycle, Can. J. Fish. Aquat. Sci., 53, 2451–2465, https://doi.org/10.1139/f96-198, 1996.